Korean J. Chem. Eng., 35(8), 1601-1610 (2018)
DOI: 10.1007/s11814-018-0068-y

pISSN: 0256-1115
eISSN: 1975-7220

A model predictive functional control based on proportional-integral-derivative (PID) and proportional-integral-proportional-derivative (PIPD) using extended non-minimal state space: Application to a molten carbonate fuel cell process

Beom Seok Kim, Tae Young Kim, Tae Chang Park, and Yeong Koo Yeo†

Department of Chemical Engineering, Hanyang University, Seoul 04763, Korea
(*Received 3 December 2017 • accepted 30 April 2018*)

Abstract−The performance of most controllers, including proportional-integral-derivative (PID) and proportional-integral-proportional-derivative (PIPD) controllers, depends upon tuning of control parameters. In this study, we propose a novel tuning strategy for PID and PIPD controllers whose control parameters are tuned using the extended non-minimal state space model predictive functional control (ENMSSPFC) scheme based on the auto-regressive moving average (ARMA) model. The proposed control method is applied numerically in the operation of the MCFC process with the parameters of PID and PIPD controllers being optimized by ENMSSPFC based on the ARMA model for the MCFC process. Numerical simulations were carried out to assess the set-point tracking performance and disturbance rejection performance both for the perfect plant model, which represents the ideal case, and for the imperfect plant model, which is usual in practical applications. When there exists uncertainty in the plant model, the PIPD controller exhibits better overall control performance compared to the PID controller.

Keywords: PID Control, PIPD Control, Extended Non-minimal State Space Model, Predictive Functional Control, Molten Carbonate Fuel Cell, Numerical Simulation

INTRODUCTION

The proportional-integral-derivative (PID) controller is a very effective control method widely adopted in many industrial processes [1]. A novel generalized predictive control (GPC) coupled with PID control method was proposed to provide similar performance as GPC and the compact structure as conventional PID controller [2]. The fuzzy control scheme was combined with PID control method to yield a new multivariable predictive fuzzy-PID control system [3]. Zhang et al. proposed a new PID controller in which the predictive functional control (PFC) scheme was combined with conventional PID control method [4].

Majhi proposed a PIPD control method which may be considered as a branch of conventional PID controller [5]. In this PIPD control method, the PD control scheme is used to improve values of the poles of the process transfer function followed by control operation using the PI controller. The PIPD control method is known to exhibit good control performance for the processes with long time delay.

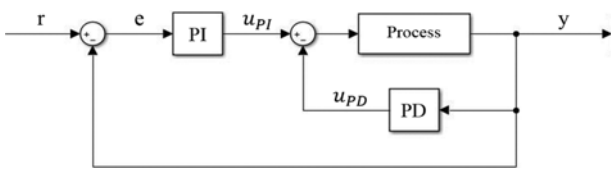

Fig. 1. Basic structure of PIPD control system.

†To whom correspondence should be addressed.
E-mail: ykyeo@hanyang.ac.kr

As shown in Fig. 1, the PIPD control system includes a PI controller in the outer loop and a PD controller in the inner feedback loop.

Practical application of the PIPD control method is not easy because the number of tuning parameters is greater than that of conventional PID controllers. A conventional PID controller includes three tuning parameters: controller gain (proportional coefficient), reset time (integral coefficient), and derivative time (differential coefficient). In contrast, a PIPD controller contains four tuning parameters: a controller gain and a reset time at the outer loop, and another controller gain and derivative time at the inner feedback loop. So far, many tuning methods have been proposed for PID controllers. Among them, the PID tuning strategies proposed by Astrom and Tyreus are based on the process reaction curve [6,7]. The PID tuning method proposed by Zhuang and Artherton employs the minimization of the integral performance criterion [8]. As for the tuning of PIPD controllers, Padhy and Majhi proposed a tuning strategy based on the gain margin criterion [9]. A tuning method using the plotting of stability boundary was proposed [10]. But these tuning methods identify fixed tuning parameters and lack an ability of countermeasure to the changes in the process states.

The extended non-minimal state space model predictive functional control (ENMSSPFC) employs the extended non-minimal state space (ENMSS) model, in which state variables and control errors are combined to determine the tuning parameters of PID and PIPD controllers at each sampling time. The ENMSS model is constructed by combination of control error and the non-minimal state space (NMSS) model. The ENMSS model is characterized by simple configuration and good control performance for plant-model mismatched processes. On the basis of these properties, ENMSSPFC combined with variable control methods has been applied to many

industrial processes. Zhang et al. suggested the PID controller using ENMSSPFC [11]. The new PID controller was used to control the chamber pressure in an industrial coke furnace, and the simulation results showed that the suggested PID controller displayed better control performance compared to other conventional PID controllers. Wu proposed the PID controller based on ENMSSPFC for multivariable processes [12]. The simulation results for chamber pressure in a coke furnace, Vinante and Luyben column system and distillation column illustrated improved control performance compared to reported results [13]. HongboZou and HaishengLi proposed a PIPD controller using ENMSSPFC for the stabilized gasoline vapor pressure [14]. By using the proposed PIPD controller, the set-point tracking and disturbance rejection performances were improved compared to other controllers for single-input single-output processes.

In this study, inspired by the ENMSS model, a predictive functional control method for multivariable processes based on PID and PIPD control schemes using ENMSSPFC is proposed and applied to a molten carbonate fuel cell (MCFC) process to evaluate the control performance of the proposed ENMSSPFC-PID and PIPD controllers.

EXTENDED NON-MINIMAL STATE SPACE MODEL

The non-minimal state space (NMSS) model consists of past input-output data and provides improved convergence rate and robustness compared to a simple state space model [15-17]. For a process with p inputs and q outputs, the difference model equation can be expressed as:

$$\begin{aligned}&\mathbf{y}(k+1)+\mathbf{L}_1\mathbf{y}(k)+\mathbf{L}_2\mathbf{y}(k-1)+\cdots+\mathbf{L}_n\mathbf{y}(k-n+1)\\&\quad=\mathbf{S}_1\mathbf{u}(k)+\mathbf{S}_2\mathbf{u}(k-1)+\cdots+\mathbf{S}_n\mathbf{u}(k-n+1)\end{aligned}\tag{1}$$

where $\mathbf{y}(k)$ and $\mathbf{u}(k)$ are output and input vector at time k, respectively, and $\mathbf{L}_1$, $\mathbf{L}_2$ … $\mathbf{L}_n$ and $\mathbf{S}_1$, $\mathbf{S}_2$ … $\mathbf{S}_n$ are q×q and q×p coefficient matrices, respectively. Introducing the back shift operator Δ defined by $\Delta\mathbf{y}(k+1)=\mathbf{y}(k+1)-\mathbf{y}(k)$ and $\Delta\mathbf{u}(k)=\mathbf{u}(k)-\mathbf{u}(k-1)$, this equation can be rewritten as

$$\begin{aligned}&\Delta\mathbf{y}(k+1)+\mathbf{L}_1\Delta\mathbf{y}(k)+\mathbf{L}_2\Delta\mathbf{y}(k-1)+\cdots+\mathbf{L}_n\Delta\mathbf{y}(k-n+1)\\&\quad=\mathbf{S}_1\Delta\mathbf{u}(k)+\mathbf{S}_2\Delta\mathbf{u}(k-1)+\cdots+\mathbf{S}_n\Delta\mathbf{u}(k-n+1)\end{aligned}\tag{2}$$

The NMSS vector $\Delta\mathbf{x}_m(k)^T$ is defined as

$$\begin{aligned}\Delta\mathbf{x}_m(k)^T=[&\Delta\mathbf{y}(k)^T,\Delta\mathbf{y}(k-1)^T,\ldots,\Delta\mathbf{y}(k-n+1)^T,\\&\Delta\mathbf{u}(k-1)^T,\Delta\mathbf{u}(k-2)^T,\ldots,\Delta\mathbf{u}(k-n+1)^T]\end{aligned}$$

where m in $\Delta\mathbf{x}_m(k)$ is defined as $m=p\times(n-1)+q\times n$. Using $\Delta\mathbf{x}_m(k)$, the state space model can be expressed as follows:

$$\begin{aligned}&\Delta\mathbf{x}_m(k+1)=\mathbf{A}_m\Delta\mathbf{x}_m(k)+\mathbf{B}_m\Delta\mathbf{u}(k)\\&\Delta\mathbf{y}(k+1)=\mathbf{C}_m\Delta\mathbf{x}_m(k+1)\end{aligned}\tag{3}$$

$$\mathbf{A}_m=\begin{bmatrix}-\mathbf{L}_1&-\mathbf{L}_2&\cdots&-\mathbf{L}_{n-1}&-\mathbf{L}_n&\mathbf{S}_2&\cdots&\mathbf{S}_{n-1}&\mathbf{S}_n\\\mathbf{I}_q&0&\cdots&0&0&0&\cdots&0&0\\0&\mathbf{I}_q&\cdots&0&0&0&\cdots&0&0\\\vdots&\vdots&\cdots&\vdots&\vdots&\vdots&\cdots&\vdots&\vdots\\0&0&\cdots&\mathbf{I}_q&0&0&\cdots&0&0\\0&0&\cdots&0&0&0&\cdots&0&0\\0&0&\cdots&0&0&\mathbf{I}_p&\cdots&0&0\\\vdots&\vdots&\cdots&\vdots&\vdots&\vdots&\vdots&\vdots&\vdots\\0&0&\cdots&0&0&0&\cdots&\mathbf{I}_p&0\end{bmatrix},$$

$$\mathbf{B}_m^T=[\mathbf{S}_1^T\ 0\ 0\ \cdots\ 0\ \mathbf{I}_p\ 0\ 0],\ \mathbf{C}_m=[\mathbf{I}_p\ 0\ 0\ \cdots\ 0\ 0\ 0\ 0]$$

The dimensions of the matrices $\mathbf{A}_m$, $\mathbf{B}_m$ and $\mathbf{C}_m$ are m×m, m×p and q×m, respectively.

An extended state variable $\mathbf{z}(k)$ is defined as

$$\mathbf{z}(k)=\begin{bmatrix}\Delta\mathbf{x}_m(k)\\\mathbf{y}(k)\end{bmatrix}\tag{4}$$

Using z(k), the previous state space model may be rewritten as

$$\begin{aligned}&\mathbf{z}(k+1)=\mathbf{A}\mathbf{z}(k)+\mathbf{B}\Delta\mathbf{u}(k)\\&\mathbf{y}(k+1)=\mathbf{C}\mathbf{z}(k+1)\end{aligned}\tag{5}$$

$$\mathbf{A}=\begin{bmatrix}\mathbf{A}_m&\underline{0}\\\mathbf{C}_m\mathbf{A}_m&\mathbf{I}_q\end{bmatrix},\ \mathbf{B}=\begin{bmatrix}\mathbf{B}_m\\\mathbf{C}_m\mathbf{B}_m\end{bmatrix},\ \mathbf{C}=[\underline{0}^T\ \mathbf{I}_q]\tag{6}$$

where $\underline{0}$ is a m×q zero matrix and $\mathbf{I}_q$ denotes a q×q identity matrix. The NMSS model and tracking errors can be combined to construct an extended non-minimal state space (ENMSS) model. The control methods based on ENMSS models may provide enhanced degree of freedom in the design of control system. The control error $\mathbf{e}(k)$ is given by

$$\mathbf{e}(k)=\mathbf{y}(k)-\mathbf{r}(k)\tag{7}$$

where $\mathbf{r}(k)$ is the reference value. Thus we have

$$\mathbf{e}(k+1)=\mathbf{y}(k+1)-\mathbf{r}(k+1)\tag{8}$$

Taking difference between these two equations, we have

$$\begin{aligned}\mathbf{e}(k+1)-\mathbf{e}(k)&=\mathbf{y}(k+1)-\mathbf{y}(k)-\mathbf{r}(k+1)+\mathbf{r}(k)\\&=\Delta\mathbf{y}(k+1)-\Delta\mathbf{r}(k+1)\end{aligned}\tag{9}$$

Substitution of Eq. (3) into Eq. (9) gives

$$\mathbf{e}(k+1)=\mathbf{e}(k)+\mathbf{C}_m\mathbf{A}_m\Delta\mathbf{x}_m(k)+\mathbf{C}_m\mathbf{B}_m\Delta\mathbf{u}(k)-\Delta\mathbf{r}(k+1)\tag{10}$$

A new extended state variable $\mathbf{z}_e(k)$ is defined as follows:

$$\mathbf{z}_e(k)=\begin{bmatrix}\Delta\mathbf{x}_m(k)\\\mathbf{e}(k)\end{bmatrix}\tag{11}$$

Using $\mathbf{z}_e(k)$, the ENMSS model can be expressed as

$$\mathbf{z}_e(k+1)=\mathbf{A}_e\mathbf{z}_e(k)+\mathbf{B}_e\Delta\mathbf{u}(k)+\mathbf{C}_e\Delta\mathbf{r}(k+1)\tag{12}$$

$$\mathbf{A}_e=\begin{bmatrix}\mathbf{A}_m&0\\\mathbf{C}_m\mathbf{A}_m&\mathrm{I}_q\end{bmatrix},\ \mathbf{B}_e=\begin{bmatrix}\mathbf{B}_m\\\mathbf{C}_m\mathbf{B}_m\end{bmatrix},\ \mathbf{C}_e=\begin{bmatrix}\underline{0}\\-\mathbf{I}_q\end{bmatrix}$$

ENMSS PREDICTIVE FUNCTIONAL CONTROL

ENMSSPFC can be implemented based on PID and PIPD controllers [18,19]. The optimal tuning parameters for PID and PIPD controllers can be determined by using the receding horizon optimization at each sampling instant. To make the calculation procedure simple, let's assume that the control horizon is 1 and calculate the future state variables using Eq. (12) as follows:

$$\mathbf{z}_e(k+P)=\mathbf{A}_e^P\mathbf{z}_e(k)+\gamma\Delta\mathbf{u}(k)+\varsigma\Delta R\tag{13}$$

$$\mathbf{z}_e(\mathrm{k+P})=\begin{bmatrix}\mathbf{z}_e(\mathrm{k+1})\\ \mathbf{z}_e(\mathrm{k+2})\\ \vdots\\ \mathbf{z}_e(\mathrm{k+P})\end{bmatrix}=\begin{bmatrix}\mathbf{A}_e\\ \mathbf{A}_e^2\\ \vdots\\ \mathbf{A}_e^P\end{bmatrix}\mathbf{z}_e+\begin{bmatrix}\mathbf{B}_e\\ \mathbf{A}_e\mathbf{B}_e\\ \vdots\\ \mathbf{A}_e^{P-1}\mathbf{B}_e\end{bmatrix}\Delta\mathbf{u}(\mathrm{k})+\begin{bmatrix}\mathbf{C}_e & 0 & 0 & \cdots & 0\\ \mathbf{A}_e\mathbf{C}_e & \mathbf{C}_e & 0 & \cdots & 0\\ \mathbf{A}_e^2\mathbf{C}_e & \mathbf{A}_e\mathbf{C}_e & \mathbf{C}_e & \cdots & 0\\ \vdots & \vdots & \vdots & \cdots & \vdots\\ \mathbf{A}_e^{P-1}\mathbf{C}_e & \mathbf{A}_e^{P-2}\mathbf{C}_e & \mathbf{A}_e^{P-3}\mathbf{C}_e & \cdots & \mathrm{C}_e\end{bmatrix}\Delta\mathrm{R} \tag{14}$$

$\varsigma=[\mathbf{A}_e^{P-1}\mathbf{C}_e\ \ \mathbf{A}_e^{P-2}\mathbf{C}_e\ \cdots\ \mathbf{C}_e]$, $\gamma=\mathbf{A}_e^{P-1}\mathbf{B}_e$

$\Delta\mathrm{R}=[\Delta\mathbf{r}(\mathrm{k+1})\ \ \Delta\mathbf{r}(\mathrm{k+2})\ \cdots\ \Delta\mathbf{r}(\mathrm{k+P})]^T$

$(\mathbf{r}(\mathrm{k+i})=\alpha^i\mathbf{y}(\mathrm{k})+(1-\alpha^i)\mathbf{c}(\mathrm{k}))$

where P is the prediction horizon, α is the smoothing factor for r, and **c**(k) is the set-point at k. The objective function to be minimized can be expressed as

$$\mathbf{J}(\mathrm{k})=\mathbf{z}_e(\mathrm{k+P})^T\mathbf{Q}_e\mathbf{z}_e(\mathrm{k+P}) \tag{15}$$

where $\mathbf{Q}_e$ denotes the weighting matrix. The formulation of the PID and PIPD controllers based on the ENMSS model can be represented in incremental form as follows:

$$\begin{aligned}\mathbf{u}_{PID}(\mathrm{k})&=\mathbf{u}(\mathrm{k-1})+K_P(\mathrm{k})(\mathbf{e}_1(\mathrm{k})-\mathbf{e}_1(\mathrm{k-1}))+K_i(\mathrm{k})\mathbf{e}_1(\mathrm{k})\\&\quad+K_d(\mathrm{k})(\mathbf{e}_1(\mathrm{k})-2\mathbf{e}_1(\mathrm{k-1}))+\mathbf{e}_1(\mathrm{k-2})\\&=\mathbf{u}(\mathrm{k-1})+\mathbf{e}_1(\mathrm{k})(K_p(\mathrm{k})+K_i(\mathrm{k})+K_d(\mathrm{k}))\\&\quad+\mathbf{e}_1(\mathrm{k-1})(-K_p(\mathrm{k})-2K_d(\mathrm{k}))+\mathbf{e}_1(\mathrm{k-2})K_d(\mathrm{k})\end{aligned} \tag{16}$$

$$\begin{aligned}\mathbf{u}_{PIPD}(\mathrm{k})&=\mathbf{u}(\mathrm{k-1})+K_P(\mathrm{k})(\mathbf{e}_1(\mathrm{k})-\mathbf{e}_1(\mathrm{k-1}))+K_i(\mathrm{k})\mathbf{e}_1(\mathrm{k})\\&\quad+K_f(\mathrm{k})(\mathbf{y}(\mathrm{k})-\mathbf{y}(\mathrm{k-1}))\\&\quad+K_d(\mathbf{y}(\mathrm{k})-2\mathbf{y}(\mathrm{k-1})+\mathbf{y}(\mathrm{k-2}))\\&=\mathbf{u}(\mathrm{k-1})+\mathbf{e}_1(\mathrm{k})(K_p(\mathrm{k})+K_i(\mathrm{k}))-\mathbf{e}_1(\mathrm{k-1})K_p(\mathrm{k})\\&\quad+(\mathbf{y}(\mathrm{k})-\mathbf{y}(\mathrm{k-1}))(-K_f(\mathrm{k})-K_d(\mathrm{k}))\\&\quad+(\mathbf{y}(\mathrm{k-1})+\mathbf{y}(\mathrm{k-2}))K_d(\mathrm{k})\end{aligned} \tag{17}$$

$\mathbf{e}_1(\mathrm{k})=\mathbf{c}(\mathrm{k})-\mathbf{y}(\mathrm{k})=[\mathrm{e}_{11}(\mathrm{k})\ \ \mathrm{e}_{12}(\mathrm{k})\ \cdots\ \mathrm{e}_{1q}(\mathrm{k})]^T$

where $\mathbf{e}_1(\mathrm{k})$ denotes the control errors for each output variables, K_P, K_i, K_d in Eq. (16) are proportional, integral and differential coefficients, respectively, and K_P, K_i, K_f, K_d in Eq. (17) are proportional and integral coefficients of the outer loop and proportional and differential coefficients of the feedback loop, respectively. Eq. (16) can be rewritten as follows:

$$\mathbf{u}_{PID}(\mathrm{k})=\mathbf{u}(\mathrm{k-1})+\mathbf{E}(\mathrm{k})^T\mathbf{w}(\mathrm{k}) \tag{18}$$

$$\mathbf{E}(\mathrm{k})=\begin{bmatrix}\mathbf{E}_1(\mathrm{k}) & 0 & \cdots & 0 & \cdots & 0\\ 0 & \mathbf{E}_2(\mathrm{k}) & \cdots & 0 & \cdots & 0\\ \vdots & \vdots & \vdots & \vdots & \vdots & \vdots\\ 0 & 0 & \cdots & 0 & \mathbf{E}_{p-1}(\mathrm{k}) & 0\\ 0 & 0 & \cdots & 0 & \cdots & \mathbf{E}_p(\mathrm{k})\end{bmatrix}$$

$\mathbf{E}_i(\mathrm{k})=[\mathrm{e}_{1i}(\mathrm{k})\ \ \mathrm{e}_{1i}(\mathrm{k-1})\ \ \mathrm{e}_{1i}(\mathrm{k-2})]^T$

$\mathbf{w}(\mathrm{k})=[\mathbf{w}_1(\mathrm{k})\ \ \mathbf{w}_2(\mathrm{k})\ \cdots\ \mathbf{w}_q(\mathrm{k})]^T$

$\mathbf{w}_i(\mathrm{k})=[\mathrm{w}_{i1}(\mathrm{k})\ \ \mathrm{w}_{i2}(\mathrm{k})\ \ \mathrm{w}_{i3}(\mathrm{k})]$

$\mathrm{w}_{i1}(\mathrm{k})=k_{pi}(\mathrm{k})+k_{ii}(\mathrm{k})+k_{di}(\mathrm{k})$,

$\mathrm{w}_{i2}(\mathrm{k})=-k_{pi}(\mathrm{k})-2k_{di}(\mathrm{k})$, $\mathrm{w}_{i3}(\mathrm{k})=k_{di}(\mathrm{k})$

Similarly, Eq. (17) can be converted into the following form:

$$\mathbf{u}_{PIPD}(\mathrm{k})=\mathbf{u}(\mathrm{k-1})+\mathbf{E}(\mathrm{k})^T\mathbf{w}(\mathrm{k}) \tag{19}$$

$$\mathbf{E}(\mathrm{k})=\begin{bmatrix}\mathbf{E}_1(\mathrm{k}) & 0 & \cdots & 0 & \cdots & 0\\ 0 & \mathbf{E}_2(\mathrm{k}) & \cdots & 0 & \cdots & 0\\ \vdots & \vdots & \vdots & \vdots & \vdots & \vdots\\ 0 & 0 & \cdots & 0 & \mathbf{E}_{p-1}(\mathrm{k}) & 0\\ 0 & 0 & \cdots & 0 & \cdots & \mathbf{E}_p(\mathrm{k})\end{bmatrix}$$

$\mathbf{E}_i(\mathrm{k})=[\mathbf{e}_{1i}(\mathrm{k})\ \ \mathbf{e}_{1i}(\mathrm{k-1})\ \ \mathbf{y}(\mathrm{k})-\mathbf{y}(\mathrm{k-1})\ \ \mathbf{y}(\mathrm{k-1})-\mathbf{y}(\mathrm{k-2})]^T$

$\mathbf{w}(\mathrm{k})=[\mathbf{w}_1(\mathrm{k})\ \ \mathbf{w}_2(\mathrm{k})\ \cdots\ \mathbf{w}_q(\mathrm{k})]^T$

$\mathbf{w}_i(\mathrm{k})=[\mathrm{w}_{i1}(\mathrm{k})\ \ \mathrm{w}_{i2}(\mathrm{k})\ \ \mathrm{w}_{i3}(\mathrm{k})\ \ \mathrm{w}_{i4}(\mathrm{k})]$

$\mathrm{w}_{i1}(\mathrm{k})=k_{pi}(\mathrm{k})+k_{ii}(\mathrm{k})$, $\mathrm{w}_{i2}(\mathrm{k})=-k_{pi}(\mathrm{k})$,

$\mathrm{w}_{i3}(\mathrm{k})=-k_{fi}(\mathrm{k})-k_{di}(\mathrm{k})$, $\mathrm{w}_{i4}(\mathrm{k})=k_{di}(\mathrm{k})$

Setting the derivative of the objective function Eq. (15) equal to zero, we can get the optimal **w**(k) as follows:

$$\mathbf{w}(\mathrm{k})=\mathbf{E}(\mathrm{k})(-(\gamma^T\mathbf{Q}_e\gamma\mathbf{E}(\mathrm{k})^T\mathbf{E}(\mathrm{k}))^{-1}\gamma^T\mathbf{Q}_e(\mathbf{A}_e^P\mathbf{z}_e(\varsigma\Delta\mathbf{R})) \tag{20}$$

Parameters for the PID and PIPD controllers can be determined from Eq. (20), but it can easily be found that **w**(k) may be infinite when the control system reaches the steady state. To prevent this unrealistic situation, it is necessary to set an error permission limitation, ε, so that the controller parameters remain as the same values as those at the previous sampling instant if the control error is less than ε:

PID parameters:

1) $|\mathrm{e}_{1i}(\mathrm{k})|\le\varepsilon$

$$\begin{cases}k_{pi}(\mathrm{k})=k_{pi}(\mathrm{k-1})\\ k_{ii}(\mathrm{k})=k_{ii}(\mathrm{k-1})\\ k_{di}(\mathrm{k})=k_{di}(\mathrm{k-1})\end{cases}$$

2) $|\mathrm{e}_{1i}(\mathrm{k})|>\varepsilon$

$$\begin{cases}k_{pi}(\mathrm{k})=-\mathrm{w}_{i2}(\mathrm{k})-2k_{di}(\mathrm{k})\\ k_{ii}(\mathrm{k})=\mathrm{w}_{i1}(\mathrm{k})-k_{pi}(\mathrm{k})-k_{di}(\mathrm{k})\\ k_{di}(\mathrm{k})=\mathrm{w}_{i3}(\mathrm{k})\end{cases}$$

PIPD parameters:

1) $|\mathrm{e}_{1i}(\mathrm{k})|\le\varepsilon$

$$\begin{cases}k_{pi}(\mathrm{k})=k_{pi}(\mathrm{k-1})\\ k_{ii}(\mathrm{k})=k_{ii}(\mathrm{k-1})\\ k_{fi}(\mathrm{k})=k_{fi}(\mathrm{k-1})\\ k_{di}(\mathrm{k})=k_{di}(\mathrm{k-1})\end{cases}$$

2) $|\mathrm{e}_{1i}(\mathrm{k})|>\varepsilon$

$$\begin{cases}k_{pi}(\mathrm{k})=\mathrm{w}_{i1}(\mathrm{k})+\mathrm{w}_{i2}(\mathrm{k})\\ k_{ii}(\mathrm{k})=-\mathrm{w}_{i2}(\mathrm{k})\\ k_{fi}(\mathrm{k})=-\mathrm{w}_{i3}(\mathrm{k})-\mathrm{w}_{i4}(\mathrm{k})\\ k_{di}(\mathrm{k})=\mathrm{w}_{i4}(\mathrm{k})\end{cases}$$

The controller parameters determined by above equations are substituted into Eq. (18) and (19) to generate input values at the instant k.

MCFC MODELING

1. Process Description

Fig. 2 shows the basic layout of the underlying MCFC process consisting of a mechanical device of control and operating fuel cell stack [20,21]. Usually water is supplied from the local municipal supply facility and flows through a water purifier. Part of the water should be discharged, although this water may be collected for additional purposes in some applications. Fuel gas is the mixture of steam and methane that is fed into the stack's reforming units and anodes. Natural gas flows through desulfurizers to remove sulfur compounds. If

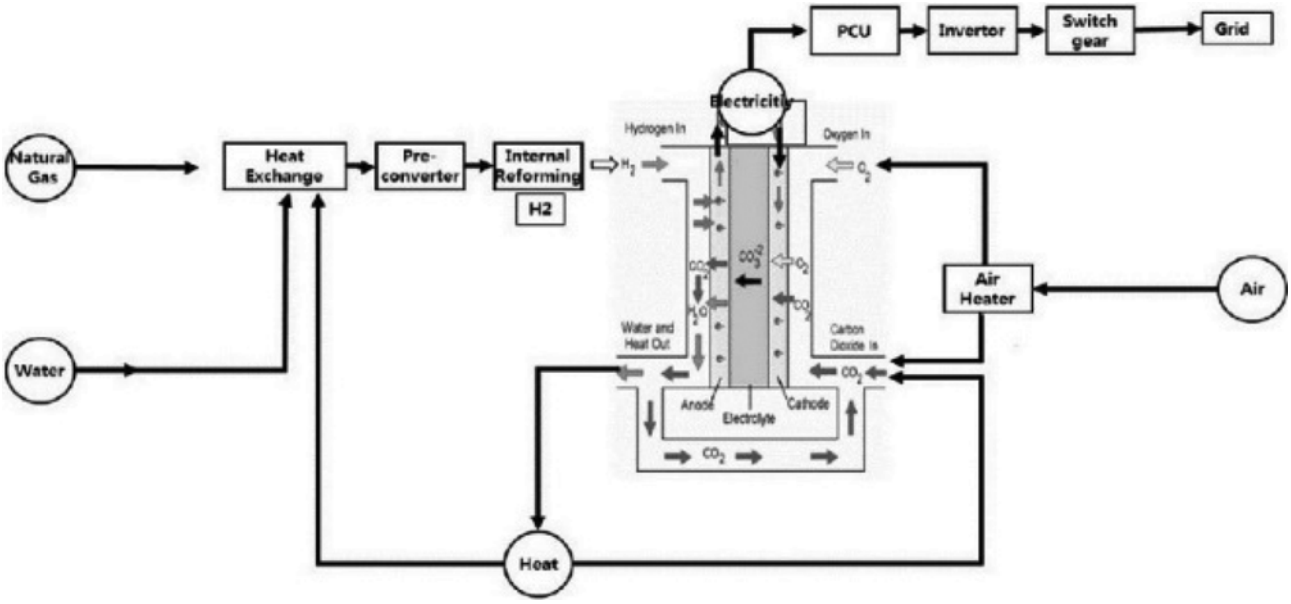

Fig. 2. Layout of the MCFC process.

these sulfur compounds are allowed to break through, they may damage the catalysts in the stack and pre-converter. The majority of the desulfurized natural gas is delivered to the humidifier where the natural gas is mixed with the purified water. Cathode exhaust gases are used to heat this mixture to yield the fuel gas. The remainder of the natural gas is provided to the air heater. The fuel gas flows through the deoxidizer and the pre-converter which contains two types of catalyst.

2. ARMA Model

The auto-regressive moving average (ARMA) model is effective in the simple interpretation of statistical time-series data and in the estimation of values for key process variables. In an auto-regression model, a linear combination of past data is used in the estimation process. An auto-regressive process model of order p can be expressed as

$$X_t=\phi_1X_{t-1}+\phi_2X_{t-2}+\ldots+\phi_pX_{t-p}+e_t \tag{21}$$

where X_t is process output at t and consists of past X values, ϕ_i are coefficient matrices, and e_t denotes the modelling error. This model is also referred to as an AR(p) model. Auto-regressive models are known to be effective to treat a wide range of various time series patterns. Rather than using past forecast variables, a moving average model employs past forecast errors given by

$$e_t=w_t+\theta_1w_{t-1}+\theta_2w_{t-2}+\ldots+\theta_qw_{t-q} \tag{22}$$

where w_t represents white noise at t and θ_i are matrices of coefficients. This model is referred to as an MA(q) model. X_t may be considered as a weighted moving average of errors of the past few forecasts. Combination of these two equations gives the model for X_t represented by ARMA (p, q) where p and q are orders of the autoregressive part and the moving average part, respectively. The ARMA model is static if the model is expressed as:

$$X_t-\phi_1X_{t-1}-\ldots-\phi_pX_{t-p}=w_t+\theta_1w_{t-1}+\ldots+\theta_qw_{t-q} \tag{23}$$

$w_t\sim WN(0, \sigma^2)$

Eq. (23) can be represented using the backshift operator defined as $z^kX_t=X_{t-k}$. Using the z operator, Eq. (23) can be rewritten as

$$\phi(z)X_t=\theta(z)w_t \tag{24}$$

where

$$\phi(z)=1-\phi_1z-\cdots-\phi_pz^p$$
$$\theta(z)=1+\theta_1z+\cdots+\theta_qz^q$$

This method is used to construct linear equations applied to time series data.

3. Fitting and Validation

Operation data on the air, water and natural gas flow rates are used in the derivation and validation of the MCFC model. In the model derivation, the hydrogen flow rates involved in the reaction are used directly instead of the natural gas flow rates. In the calculation of the hydrogen flow rates, it is assumed that 99% of the natural gas in the reformer is converted to hydrogen. In this work, 8,411 operation data of the 2.2 MW MCFC process are used to construct the MCFC model equation. The range of power is 0 to 2.2 MW. Each range of the input data including the air, water and hydrogen flow rates is 4333-6970, 1459-6747 and 331-699 SCFM, respectively. To reduce the difference of the data set scale, all data sets were preprocessed and scaled within the range [0, 1]. Fig. 3 shows the preprocessed air, hydrogen, water flow rates and the power values for the underlying 2.2 MW MCFC process.

By using the least-squares method, we can easily obtain the ARMA model given by Eq. (25). In this equation, the air, hydrogen and water flow rates are taken as manipulated variables (u_1, u_2, u_3) and the power (y) is taken as a control variable to give the linear relation:

$$\begin{aligned}y_k=&0.1174-0.0543*u_1(k-1)-0.0239*u_1(k-2)+0.1214*u_1(k-3)\\&+1.331*u_2(k-1)-0.7857*u_2(k-2)+0.4815*u_2(k-3)\\&-0.4673*u_3(k-1)+0.1479*u_3(k-2)+0.1238*u_3(k-3)\end{aligned} \tag{25}$$

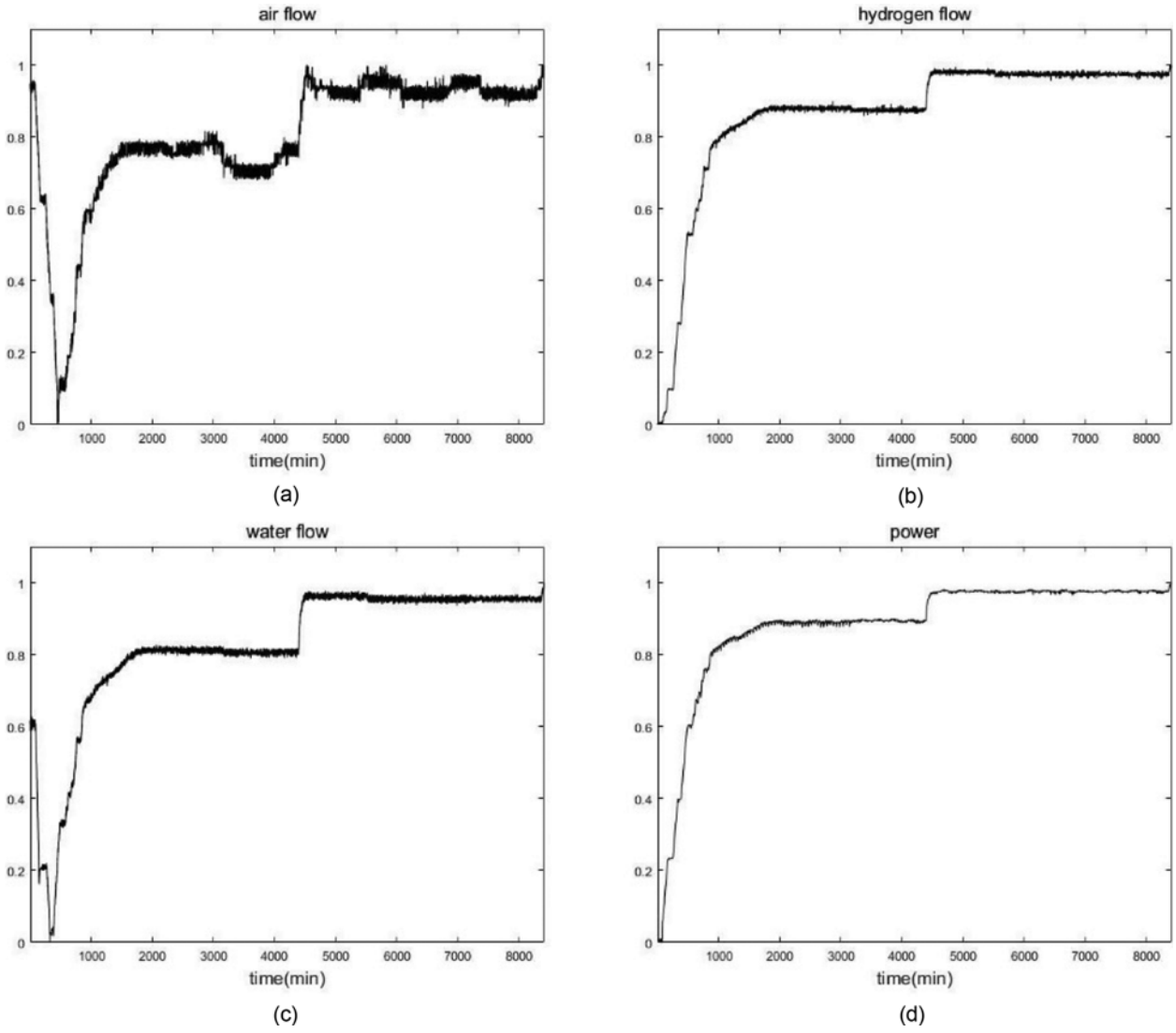

Fig. 3. Preprocessed operation data for 2.2 MW MCFC process: (a) Air flow rates, (b) hydrogen flow rates, (c) water flow rates, (d) power output.

To confirm the accuracy of the Eq. (25), the root mean square error (RMSE) defined by Eq. (26) is calculated using the operation data and the predicted valuesobtained from the Eq. (25).

$$\mathrm{RMSE} = \sqrt{\frac{\Sigma(y_k - y_{ref})^2}{N}} \tag{26}$$

where y_{ref} is operation data and N is the sample number. The RMSE value of the operation data in the model expression and the predicted value is 0.0083 and max residual is 0.103 MW. Fig. 4 shows the operation data and the predicted values.

To validate the model equation, two different data sets were prepared. First data set was composed of plant data of different time zones. The range of the data set for 4323 minutes is 0 to 2.0 MW. Second data set was composed of plant data obtained during 3355 minutes from the MCFC plant. The range of the second data set is 0 to 2.5 MW. Fig. 5 represents the predicted value from Eq. (25) and two operation data sets.

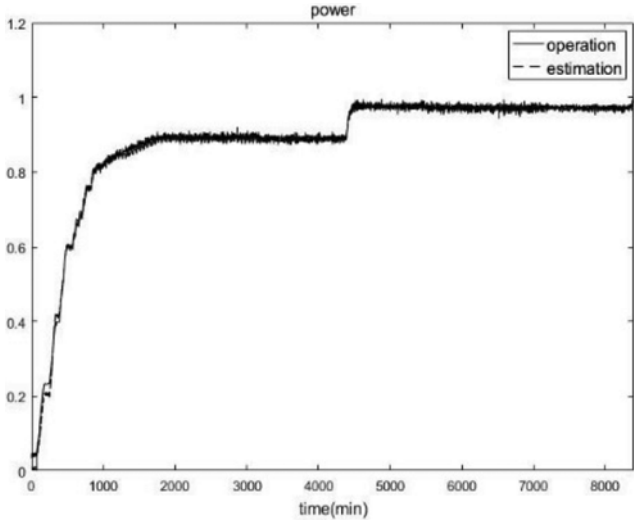

Fig. 4. Fitting of model equation.

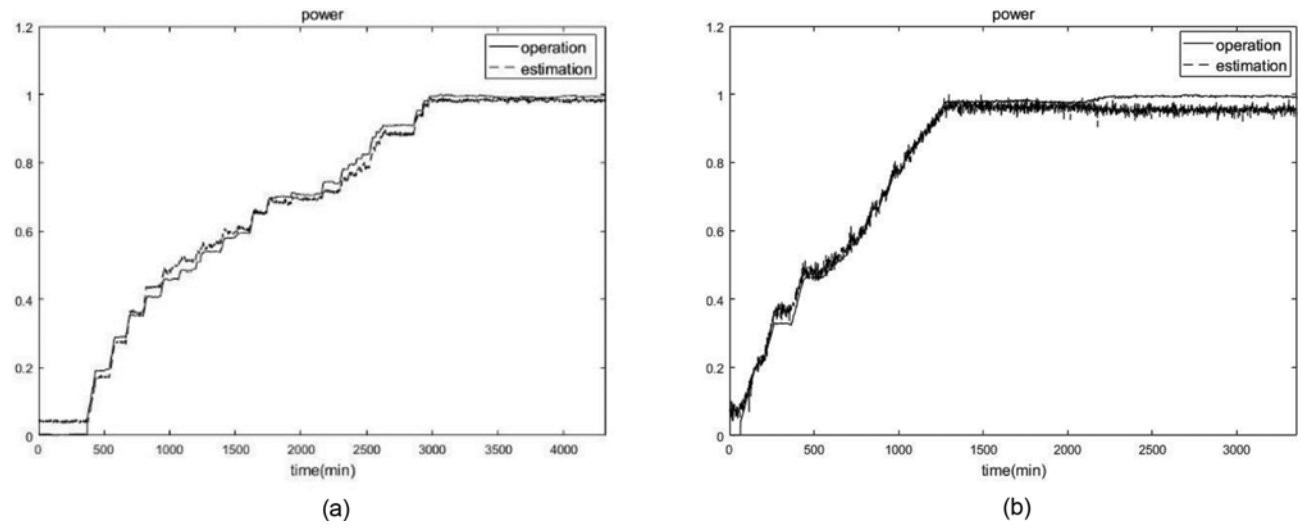

Fig. 5. Validation of model equation: (a) Different time data, (b) different plant data.

Table 1. The RMSE and maximum residual of the fitting and validation data

	Fitting data	Different time data	Different plant data
RMSE	0.0083	0.0222	0.0306
Max residual (MW)	0.103	0.112	0.252

The values of RMSE for each data set are 0.0222 and 0.0306, respectively. The maximum residual are 0.112 MW and 0.252 MW. These values are summarized in Table 1. Comparing the values of RMSE and residual, different time data is more accurate than different plant data. This is because the condition obtained from the different time data is the same as that obtained from the fitting data. Though different plant data error is larger than that of different time data, it is small enough and we can see that Eq. (25) has sufficient accuracy under different conditions. From the fitting and validation results, Eq. (25) could predict the power of a typical MCFC plant well.

CASE STUDIES

1. Perfect Plant Model

The ENMSSPFC scheme based on the ARMA model for the MCFC plant was used to implement and to compare the PID and PIPD controllers. Numerical simulations were carried out for 100 sampling instants. The set-point was set to 1 and a disturbance of magnitude −0.1 was introduced at the sampling instant of 50 to assess load rejection performance. Tables 2 and 3 show controller parameters used in the simulations. When the prediction horizon, P, is greater than 4, RMSE tends to increase. In the simulations, we set P value to 3. The smoothing factor, α, is determined by using the bisection method. The initial search interval of [0~1] was used to get 0.59 and 0.66 for PID and PIPD controllers, respectively. Q_e may be regarded as a tuning parameter matrix. While Q_e is determined by trial and error in this study, identification of a systematic selection procedure for Q_e is desirable and remains as a further study. The range of the parameter is set to [0 1] and simulations for various variables in this range are performed. In Table 2, ε denotes the error permission limitation.

Table 2. Tuning parameters for the PID controllers

	ENMSSPFC-PID
P	3
$\mathbf{Q}_e$	diag(0.2, 0.2, 0.2, 0.2, 0.2, 0.2, 0.2, 0.2, 0.2, 0.2)
α	0.59
ε	10^{-5}

Table 3. Tuning parameters for the PIPD controllers

	ENMSSPFC-PIPD
P	3
$\mathbf{Q}_e$	diag(0.2, 0.2, 0.2, 0.2, 0.2, 0.2, 0.2, 0.2, 0.2, 0.2)
α	0.66
ε	10^{-5}

Based on the ENMSS model, we have the following relations:

$$\Delta\mathbf{x}_m(k+1)^T=\mathbf{A}_m\Delta\mathbf{x}_m(k)+\mathbf{B}_m\Delta\mathbf{u}(k)$$
$$\Delta\mathbf{y}(k+1)=\mathbf{C}_m\Delta\mathbf{x}_m(k+1) \quad (27)$$

With

$$\mathbf{A}_m=\begin{bmatrix} 0 & 0 & 0 & -0.0239 & -0.7857 & 0.1479 & 0.1214 & 0.4815 & 0.1238 \\ 1 & 0 & 0 & 0 & 0 & 0 & 0 & 0 & 0 \\ 0 & 1 & 0 & 0 & 0 & 0 & 0 & 0 & 0 \\ 0 & 0 & 0 & 0 & 0 & 0 & 0 & 0 & 0 \\ 0 & 0 & 0 & 0 & 0 & 0 & 0 & 0 & 0 \\ 0 & 0 & 0 & 0 & 0 & 0 & 0 & 0 & 0 \\ 0 & 0 & 0 & 1 & 0 & 0 & 0 & 0 & 0 \\ 0 & 0 & 0 & 0 & 1 & 0 & 0 & 0 & 0 \\ 0 & 0 & 0 & 0 & 0 & 1 & 0 & 0 & 0 \end{bmatrix}$$

$$\mathbf{B}_m=\begin{bmatrix} -0.0543 & -1.3310 & -0.4673 \\ 0 & 0 & 0 \\ 0 & 0 & 0 \\ 1 & 0 & 0 \\ 0 & 1 & 0 \\ 0 & 0 & 1 \\ 0 & 0 & 0 \\ 0 & 0 & 0 \\ 0 & 0 & 0 \end{bmatrix},$$

$$\mathbf{C}_m=[1\ 0\ 0\ 0\ 0\ 0\ 0\ 0\ 0]$$

Based on these equations, we have

$$\mathbf{z}(k+1)=\mathbf{A}\mathbf{z}(k)+\mathbf{B}\Delta\mathbf{u}(k) \quad (28)$$
$$\mathbf{y}(k+1)=\mathbf{C}\mathbf{z}(k+1)$$

and the ENMSS model can be represented as:

$$\mathbf{z}_e(k+1)=\mathbf{A}_e\mathbf{z}_e(k)+\mathbf{B}_e\Delta\mathbf{u}(k)+\mathbf{C}_e\Delta\mathbf{r}(k+1)$$

$$\mathbf{A}_e=\begin{bmatrix} 0 & 0 & 0 & -0.0239 & -0.7857 & 0.1479 & 0.1214 & 0.4815 & 0.1238 \\ 1 & 0 & 0 & 0 & 0 & 0 & 0 & 0 & 0 \\ 0 & 1 & 0 & 0 & 0 & 0 & 0 & 0 & 0 \\ 0 & 0 & 0 & 0 & 0 & 0 & 0 & 0 & 0 \\ 0 & 0 & 0 & 0 & 0 & 0 & 0 & 0 & 0 \\ 0 & 0 & 0 & 1 & 0 & 0 & 0 & 0 & 0 \\ 0 & 0 & 0 & 0 & 0 & 0 & 0 & 0 & 0 \\ 0 & 0 & 0 & 0 & 1 & 0 & 0 & 0 & 0 \\ 0 & 0 & 0 & 0 & 0 & 1 & 0 & 0 & 0 \\ 0 & 0 & 0 & 0 & -0.0239 & -0.7857 & 0.1479 & 0.1214 & 0.1238 \end{bmatrix}$$

$$\mathbf{B}_e=\begin{bmatrix} -0.0543 & -1.3310 & -0.4673 \\ 0 & 0 & 0 \\ 0 & 0 & 0 \\ 1 & 0 & 0 \\ 0 & 1 & 0 \\ 0 & 0 & 1 \\ 0 & 0 & 0 \\ 0 & 0 & 0 \\ 0 & 0 & 0 \\ -0.0543 & -1.3310 & -0.4673 \end{bmatrix},$$

$$\mathbf{C}_e^T=[0\ 0\ 0\ 0\ 0\ 0\ 0\ 0\ 0\ -1]$$

Fig. 6 shows results of numerical simulations of closed-loop responses of ENMSSPFC-PID and PIPD controllers for perfect plant models. The normalized input and output values are restored to the original scales through the post treatment process. The units of output and input are MW and SCFM, respectively. In both controllers, the root mean square error (RMSE) between set-points and output values shows little discrepancy. Recovery time from the disturbance introduced at time 50 is fast and there are no oscillations and overshoots. For the perfect plant model, both controllers exhibit good tracking performance as well as excellent disturbance rejection performance.

Up-down step changes in set-point were used to verify the stability of the ENMSSPFC-PID and PIPD controllers described above. The results of simulations for these cases are shown in Fig. 7. It can be seen that ENMSSPFC-PID and PIPD can be stably applied for all operation range (0-2.2 MW).

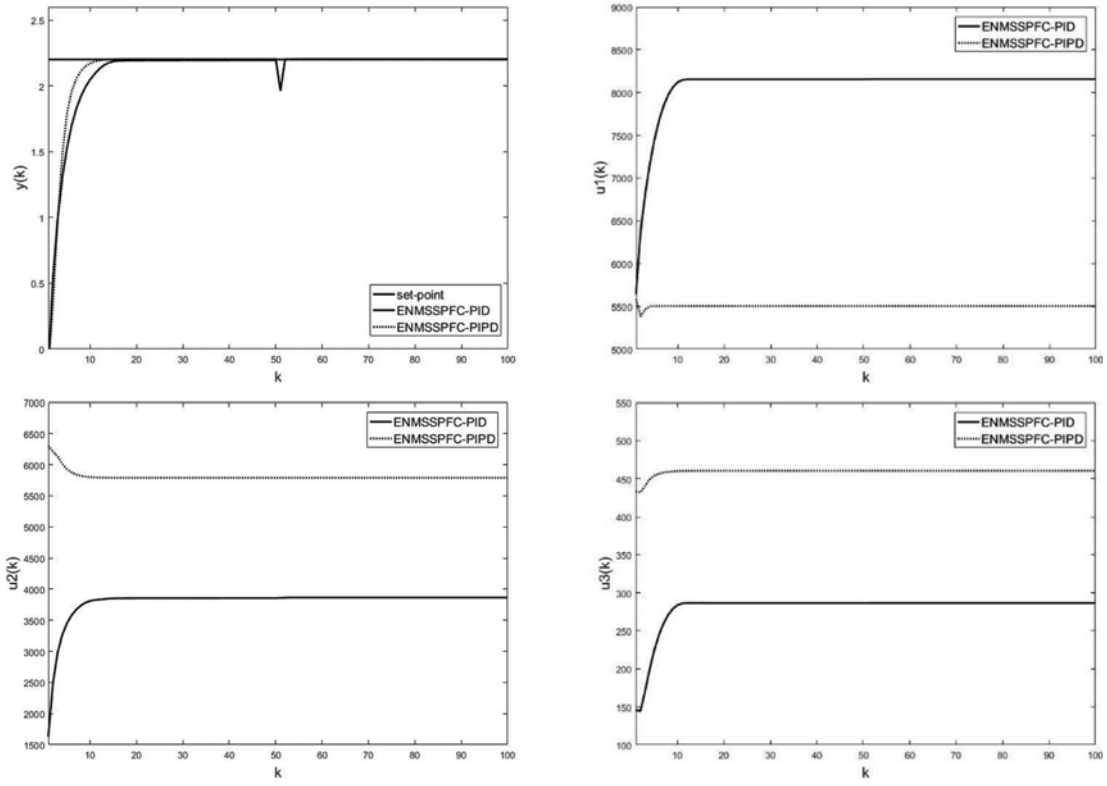

Fig. 6. Closed-loop responses of ENMSSPFC-PID and PIPD controllers: Perfect plant model.

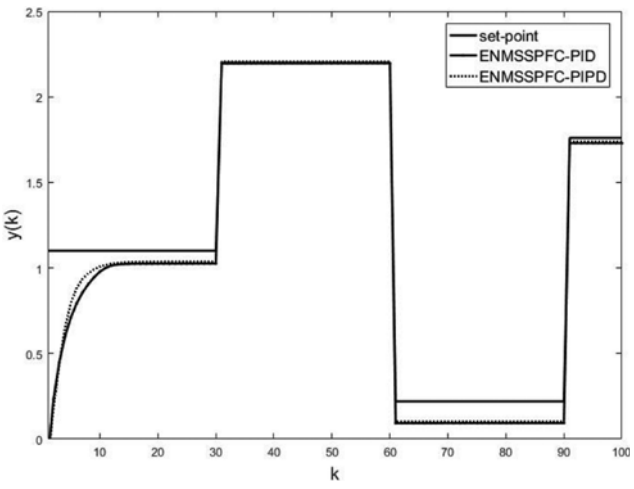

Fig. 7. Closed-loop responses of ENMSSPFC-PID and PIPD for up-down step.

2. Plant-model Mismatched

To incorporate the imperfect plant model that may be caused by the uncertainty existing in practical applications, we assumed the maximum of 20% random deviation from the parameters of the ARMA model equation and constructed three different imperfect models (cases 1, 2 and 3 as shown below) [22,23].

Table 4. RMSE of output for each case

	RMSE	
	ENMSSPFC-PID	ENMSSPFC-PIPD
Matched case	0.3393	0.3346
Mismatched: case1	0.4120	0.3228
Mismatched: case2	0.4021	0.3277
Mismatched: case3	0.4401	0.3263

Case 1:

$$y_k = 0.1174 - 0.0611 * u_1(k-1) - 0.0225 * u_1(k-2) + 0.1270 * u_1(k-3) + 1.1945 * u_2(k-1) - 0.6903 * u_2(k-2) + 0.4764 * u_2(k-3) - 0.5475 * u_3(k-1) + 0.1332 * u_3(k-2) + 0.1165 * u_3(k-3)$$

Case 2:

$$y_k = 0.1174 - 0.0615 * u_1(k-1) - 0.0279 * u_1(k-2) + 0.1337 * u_1(k-3) + 1.3764 * u_2(k-1) - 0.7184 * u_2(k-2) + 0.4585 * u_2(k-3) - 0.4766 * u_3(k-1) + 0.1631 * u_3(k-2) + 0.1272 * u_3(k-3)$$

Case 3:

$$y_k = 0.1174 - 0.0451 * u_1(k-1) - 0.0266 * u_1(k-2) + 0.1247 * u_1(k-3) + 1.0935 * u_2(k-1) - 0.9221 * u_2(k-2) + 0.4756 * u_2(k-3) - 0.4731 * u_3(k-1) + 0.1260 * u_3(k-2) + 0.0996 * u_3(k-3)$$

For each uncertain model, ENMSSPFC-PID and PIPD system were

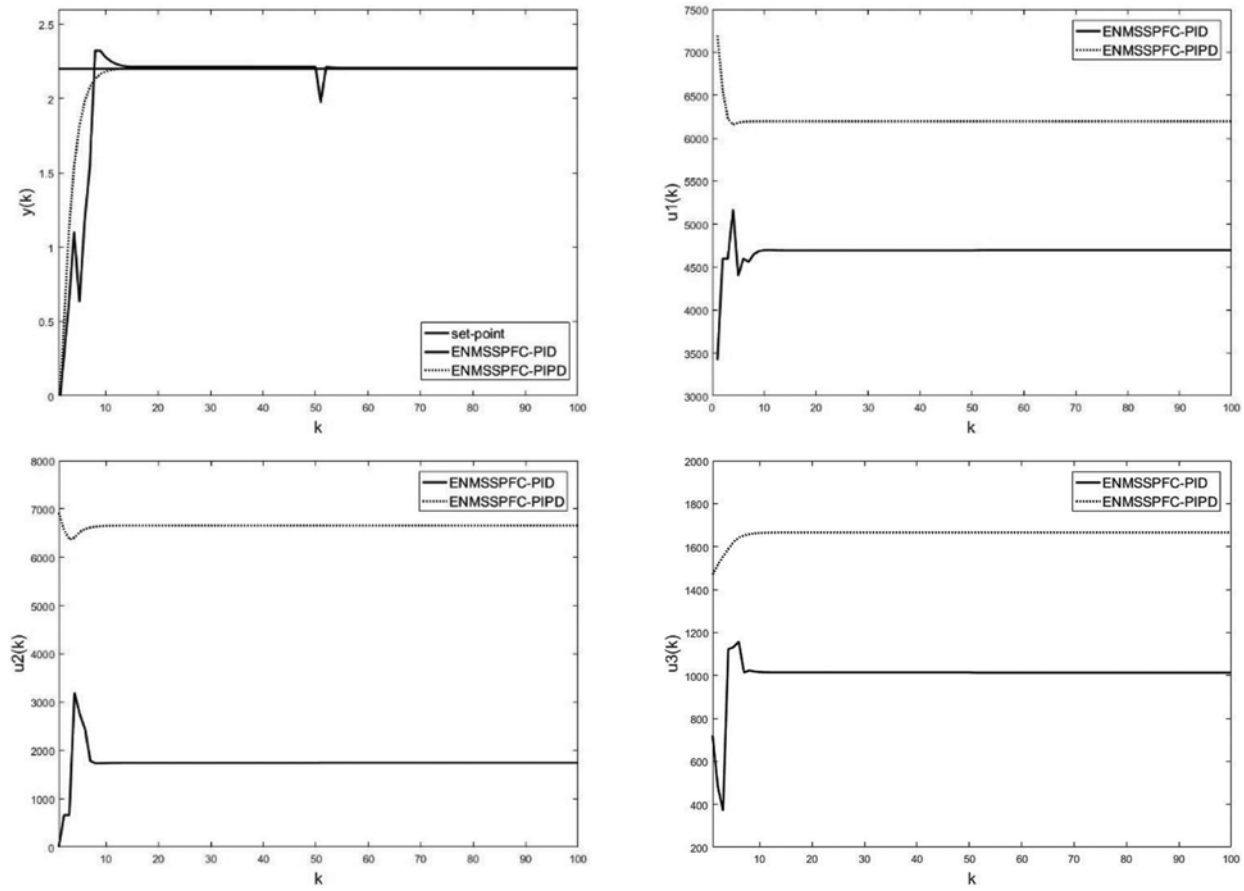

Fig. 8. Closed-loop responses of ENMSSPFC-PID and PIPD: Case 1.

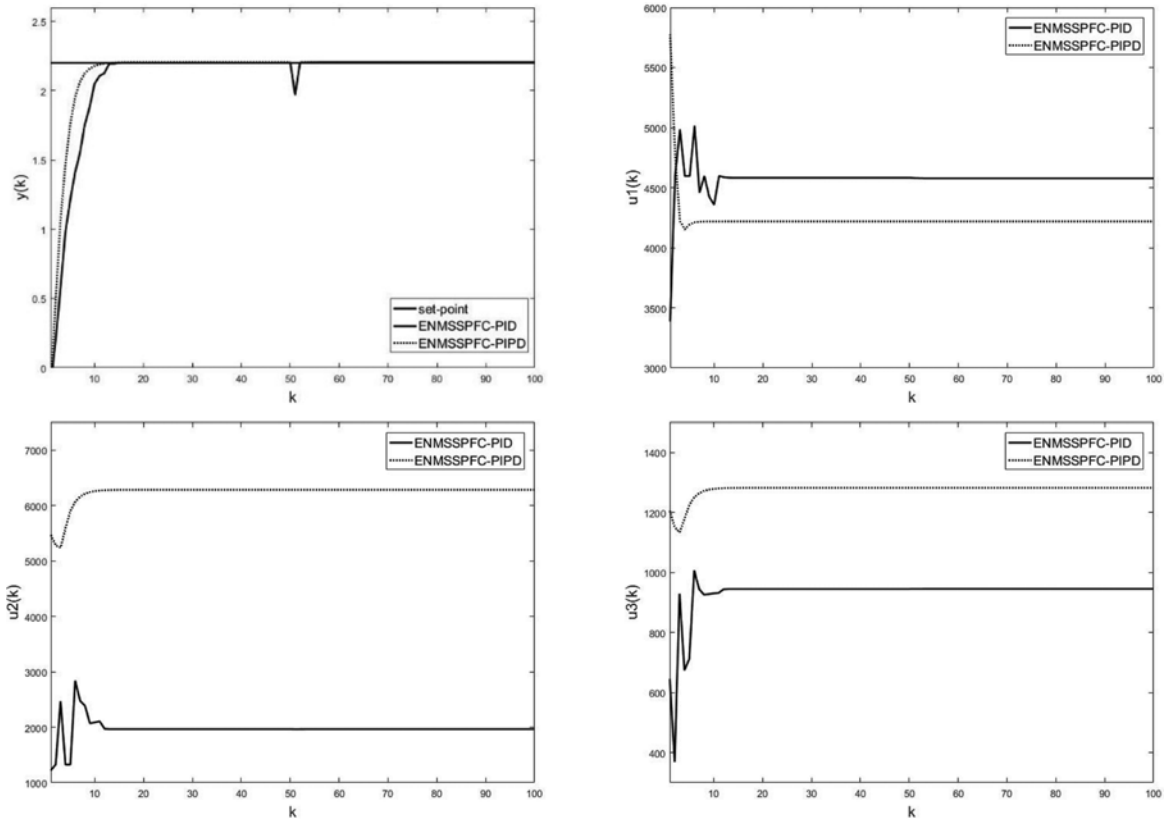

Fig. 9. Closed-loop responses of ENMSSPFC-PID and PIPD: Case 2.

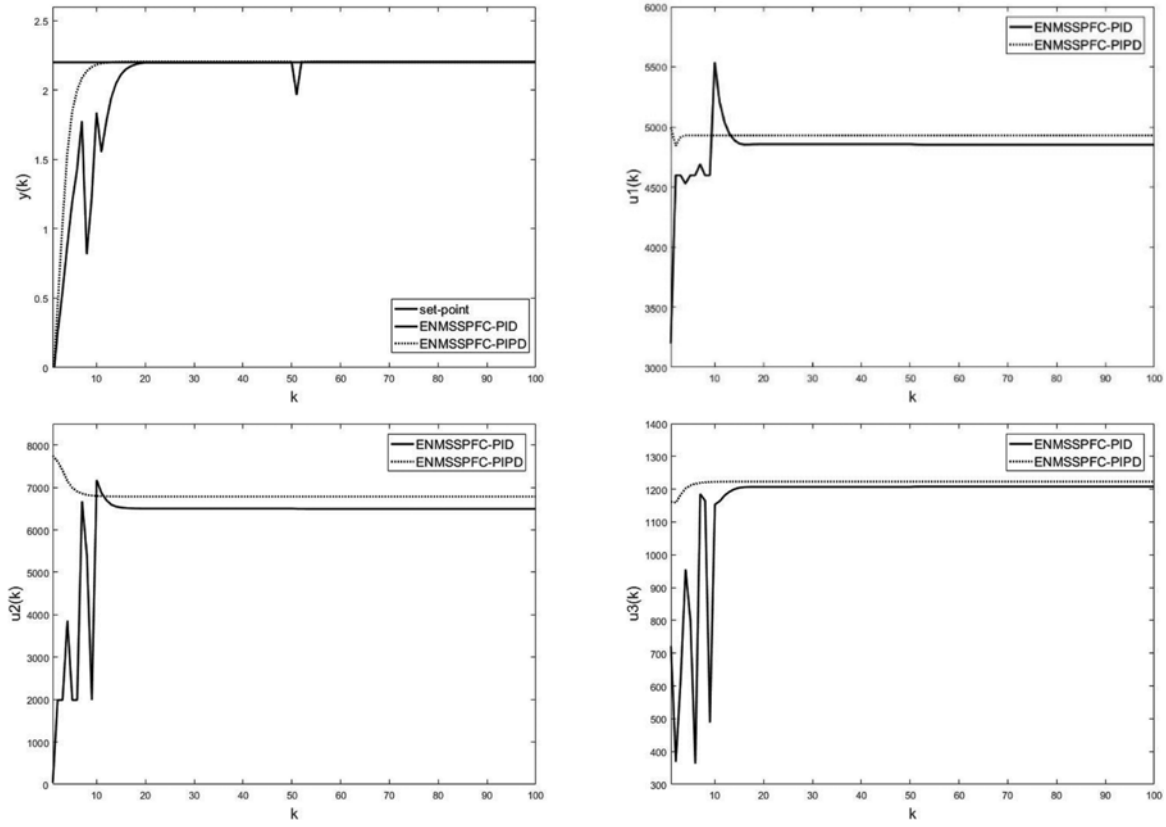

Fig. 10. Closed-loop responses of ENMSSPFC-PID and PIPD: Case 3.

constructed and numerical simulations were carried out. Results of numerical simulations are shown in Fig. 8, 9 and 10. Table 4 shows the value of the RMSE for each case.

As can be seen in Figs. 8, 9 and 10, the ENMSSPFC-PIPD controller exhibits better overall control performance than the ENMSSPFC-PID controller in all cases. Values of RMSE of the PID controller for perfect model show significant difference compared to those for the plant model mismatched cases in contrast to those of the ENMSSPFC-PIPD. Overall, the PIPD controller optimized by ENMSSPFC shows better set-point tracking and disturbance rejection performances. When the plant model is imperfect, which is usual in practical applications, we can see that the PID controller shows oscillations at the input and output. Especially, u2 and u3 in case3 go up and down from the lowest value to highest value. During the short operating time, these oscillations could add load to operation units. Thus the PIPD controller is preferred in practical applications. The PD feedback of the PIPD controller moves the poles of the process transfer function to more desirable locations. Because of this, the ENMSSPFC-PIPD controller optimizes the input to yield satisfactory output even with deviations in the process model coefficients.

CONCLUSIONS

PID and PIPD controllers optimized by ENMSSPFC based on the ARMA model are proposed for the MCFC plant. The proposed controller inherits the simple structure as conventional PID controller and the improved state space model. Numerical simulations were carried out to assess the set-point tracking performance as well as disturbance rejection performance. If the plant model is perfect, the PID controller shows the same tracking performance compared to the PIPD controller. But, when there exists uncertainty in the plant model, the PIPD controller exhibits better overall control performance than the PID controller. The PIPD controller also exhibits more fast response time and less RMSE compared to other controllers. The case studies represents the improved performance of the PIPD controller for imperfect plant models.

ACKNOWLEDGEMENTS

This work was supported by Korea Research Foundation Grant funded by the Korean Government (NRF-2017R1A2B1005649).

REFERENCES

1. R. Tchamna and M. Lee, *Korean J. Chem. Eng.*, **34**(4), 961 (2017).
2. M. Xu, S. Li and W. Cai, *Ind. Eng. Chem. Res.*, **44**(8), 2848 (2005).
3. A. Savran, *Appl. Soft Comput.*, **13**(5), 2658 (2013).
4. R. D. Zhang, P. Li, Z. Ren and S. Wang, 2009 IEEE International Conference on Control and Automation, New Zealand, Christchurch, 314 (2009).
5. S. Majhi, Ph.D. Dissertation Univ. of Sussex, Brighton, UK (1999).
6. K. J. Astrom and T. Hagglund, Instrument Society of America, Research Triangle Park, NC (1995).
7. B. D. Tyreus and W. L. Luyben, *Ind. Eng. Chem. Res.*, **31**, 2625 (1992).
8. M. Zhuang and D. P. Artherton, *IEEE Proc.-D: Control Theory Appl.*, **140**(3), 216 (1993).
9. P. K. Padhy and S. Majhi, *Comput. Chem. Eng.*, **30**(5), 790 (2006).
10. K. I. Tsai and C. C. Tsai, Proceedings of the 9th World Congress on Intelligent Control and Automation, IEEE, Taipei, Taiwan, 535 (2011).
11. R. D. Zhang, Z. X. Cao, P. Li and F. R. Gao, *IET Control Theory*, **8**(14), 1303 (2014).
12. S. Wu, *Ind. Eng. Chem. Res.*, **53**, 5505 (2015).
13. S. Wu, *Chemometrics and Intelligent Laboratory Systems*, **143**, 16 (2015).
14. H. Zou and H. Li, *Chemometrics and Intelligent Laboratory Systems*, **142**, 1 (2015).
15. A. H. Gonzalez, J. M. Perez and D. Odloak, *J. Process Control*, **19**(3), 473 (2009).
16. L. Wang and P. C. Young, *J. Process Control*, **16**, 355 (2006).
17. R. Zhang, Z. Cao, C. Bo, P. Li and F. Gao, *Ind. Eng. Chem. Res.*, **53**, 3283 (2014).
18. L. Wang, *J. Process Control*, **14**, 131 (2004).
19. R. D. Zhang, A. K. Xue, S. Q. Wang and Z. Y. Ren, *J. Process Control*, **21**(8), 1183 (2011).
20. J. H. Hirschenhofer, D. B. Stauffer, R. R. Engleman and M. G. Klett, U.S. Department of Energy Office of Fossil Energy Federal Energy Technology Center, Morgantown (1998).
21. A. Permatasari, P. Fasahati, J. H. Ryu and J. J. Liu, *Korean J. Chem. Eng.*, **33**(12), 3381 (2016).
22. J. Zhang, *Ind. Eng. Chem. Res.*, **52**, 4874 (2013).
23. R. Zhang and F. Gao, *Ind. Eng. Chem. Res.*, **52**, 817 (2013).